Study of Localization Estimation of Abasic Sites in DNA Irradiated with Ionizing Radiation

K. Akamatsu, N. Shikazono and T. Saito[1]

Irreparable DNA Damage Analysis Research Group, Quantum Beam Science Research Center, Japan Atomic Energy Agency (JAEA)
[1]Research Reactor Institute, Kyoto University

INTRODUCTION:

DNA lesions induced by ionizing radiation and chemicals can cause mutation and carcinogenesis. In particular, "clustered damage" site, that is a DNA region with multiple lesions within one or two helical turns, is believed to hardly be repaired. This damage is considered to be induced, *e.g.*, around high-LET ionizing radiation tracks. However, detail of the damage is not known. We have already developed a method for estimating degree of localization of abasic sites (APs) in DNA using Förster resonance energy transfer occurred between different fluorescence probes ("hetero-FRET" using Alexa350 and Alexa488) [1] . The results showed that $^{12}C^{5+}$ beam produced close APs within a track: the apparent distance calculated was approximately 17 base pairs [2]. This finding indicates that *direct radiation effect* of $^{12}C^{5+}$ beam near the Bragg peak produces clustered DNA damage. We have recently applied the method to DNA in a cell-mimetic radical scavenging condition [3,4]. However, there are some problems of the complex protocol and of the sensitivity due to the low extinction coefficient of Alexa350. We have, therefore, developed "homo-FRET" occurred between two or more Alexa488 molecules. We will obtain magnitude of FRET also from "fluorescence anisotropy" of homo-FRET between Alexa488 molecules. The new protocol using homo-FRET enables us to estimate DNA damage localization without any enzymes and improves sensitivity to detect a clustered damage.

EXPERIMENTS:

●*Sample preparation and γ-irradiation*

The plasmid DNA digested by Sma I was used (linear form). The DNA was dissolved to be 0.1 g/L in 0.2 M Tris-HCl buffer (pH 7.5) which is a cell-mimetic condition in relation to radical scavenging capacity. Twenty microliters of the DNA solution was transferred to a microtube (0.5-mL size), and was irradiated with ^{60}Co γ-rays (LET: ~0.2 keV/μm; Kyoto University Research Reactor Institute: KURRI) as a standard radiation source.

●*Preparation of fluorophore-labeled irradiated DNA and the FRET observation*

The irradiated DNA (10 μL in water) and 10 μL of 100 mM Tris-HCl (pH 7.5) were mixed in a microtube. Two microliters of Alexa488/DMSO was added to the DNA solution and was incubated for 24 h at 35°C. The fluorophore-labeled DNA was purified by ethanol-precipitation followed by ultrafiltration. The fluorescence anisotropy was measured at 525 nm (ex. 470 nm).

The anisotropy, $< r >$, is defined as follows:

$$< r > = \frac{I_{VV} - G \bullet I_{VH}}{I_{VV} + 2G \bullet I_{VH}},$$

where I_{VV} is the fluorescence intensity when the excitation and emission polarizers are both vertically oriented. I_{VH} is one when the excitation/emission polarizers are vertically/horizontally oriented. G is the grating factor defined as I_{HV}/I_{HH}.

RESULTS AND DISCUSSION:

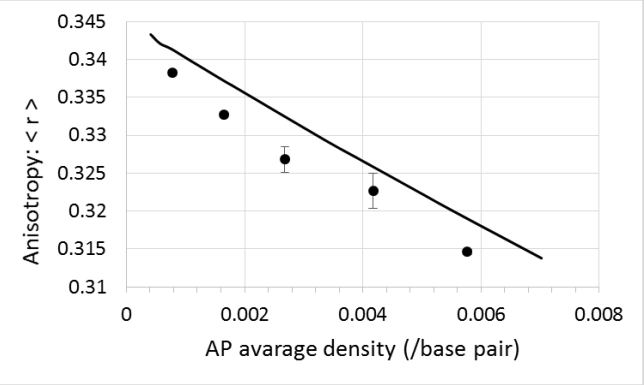

Fig. 1. Relationship between AP average density (the number of APs per base pair) and fluorescence anisotropy for ^{60}Co γ-rays (●). The solid line indicates a theoretical curve for Poisson distributed APs in DNA.

In general, fluorescence anisotropy decreases with increasing FRET [5]. As shown in Fig.1, there was a little difference between the γ-ray data points and a theoretical curve based on Poisson distribution. This finding suggest that APs produced by the γ-rays are likely to be localized compared to those randomly distributed. This tendency is similar to the hetero-FRET results as shown previously [2-4]. A radiation "spur" on or nearby DNA might sometimes produces clustered damage. In any case, knowledge of AP distribution for ^{60}Co γ-rays *as a reference* is quite important to study DNA damage by ionizing radiation.

REFERENCES:

[1] K. Akamatsu, N. Shikazono, Anal. Biochem. **433** (2013) 171-180.
[2] K. Akamatsu, N. Shikazono, and T. Saito, Radiat. Res. **183** (2015) 105-113.
[3] K. Akamatsu, N. Shikazono, and T. Saito, KURRI Progress Report 2012 (2013) 263.
[4] K. Akamatsu, N. Shikazono, and T. Saito, KURRI Progress Report 2014 (2014) 127.
[5] L. W. Runnels, and S. F. Scarlata, Biophys. J. **69** (1995) 1569.

CO6-2 Structural Insights of the Degradation Scheme of Yeast 20S Proteasome Studied by Genetic Mutation and AFM Motion Imaging

H.Yamaguchi[1],T.Amako[1], M.Unno[2], I.Hisatome[3], K.Hosokawa[1] and Y.Morimoto

Research Reactor Institute, Kyoto University
[1]School of Science and Technology, Kwansei Gakuin University
[2]Graduate School of Science and Engineering, Ibaraki University
[3]Institute of Regenerative Medicine and Biofunction, Tottori University

INTRODUCTION: Proteasomes are the multicatalytic protein complexes with large molecular weight. It is well known that the ubiquitin proteasome system plays an important role in regulated proteolysis. Proteasome works as 26S particle that is composed of two 19S regulating components and a 20S proteasome. The 20S proteasome forms barrel shape and is composed of four rings, α- and β-rings; each ring contains highly homological seven α- and seven β-subunits. Each of 1, 2 and 5 β-subunit has different enzyme activity; 1 is caspase-, 2 tryptic- and 5 chymotryptic- like activity, respectively. It was found recently that inhibition of 20S proteasome activity resulted in decrease and disappearance of cancer cells. The complex structure of 20S proteasome and its inhibitor have been determined by X-ray diffraction method. Binding site of inhibitor is closed to Tyr170 and Thr1 of the β5 subunit. It is considered that an aromatic ring of the inhibitor interacts with Y170 by ring-stacking force. Since weak interaction of compounds to active amino acid residues we found, processing or degradation assay have been clarified by use of genetic mutations of the yeast 20S proteasome. Tyrosine mutations to Ala, Phe and Leu may not have interaction with the inhibitor and strictly changes binding activities to the 19S particle. The whole particle, 26S proteasome, including such 20S core is very important in the actual living cell for a degradation or stabilization on the cell circulation. Especially, a motion or behavior of the 26S proteasome when a regulatory particles bound should be clarified at atomic- or nano-scale resolution, we have tried to visualize such behavior as a motion capture of the atomic force microscopy (AFM) technique.

EXPERIMENTS: Yeast 20S (wild, and genetic modifications in the β5 subunit; Y170A, Y170L and Y170F) and 26S proteasome particles were prepared by using yeast (*Saccharomyces cerevisiae*) cell cultivated. The crude extract was purified by using M2 affinity and Mono-Q anion exchange chromatography techniques. When the 26S particle was isolated, gel filtration chromatography was continuously applied with a buffer solution including ATP. Isolated 20S proteasome was concentrated by ultrafiltration. Activity measurement of wild and mutant proteasomes in the presence of the inhibitor was carried out in order to reinvestigate the inhibition mechanism. AFM images of the 26S proteasome were measured by NanoExplorer at 20°C at the Research Institute of Biomolecule Metrology in Tsukuba. Particle analysis was carried out by AFM reconstitution.

RESULTS: Genetic mutation for Y170 would have activities because of a lack of aromatic ring in the amino acid residue in the Ala and Leu, binding ability of the inhibitor might be lost. Typical activity assay for wild-type 20S shows reduction, otherwise the Y170L has no decrease of activity assay. Since additive order or combination of substrates and inhibitors affects hydrolysis strongly, 26S whole particle may have specific character in terms of own-shape.

The AFM measurement shows whole structure of the 26S particle, and analyses of resultant images describe a shape and size, and also a structural motion. Intensity distribution analysis, which reconstitutes outer shape of particle by enormous amount of omnidirectional image data, was applied for the AFM image that is able to judge as 26S proteasome. Intensity distribution of AFM data (Figure 1a) shows symmetrical shape, which is consistent with the size and shape of a double-capped whole 26S particle composed of central 20S and the both ends (Figure 1b). Measurements of AFM images of proteasome in the presence of substrates are in progress in order to analyze dynamic motion when proteasome is working.

a)

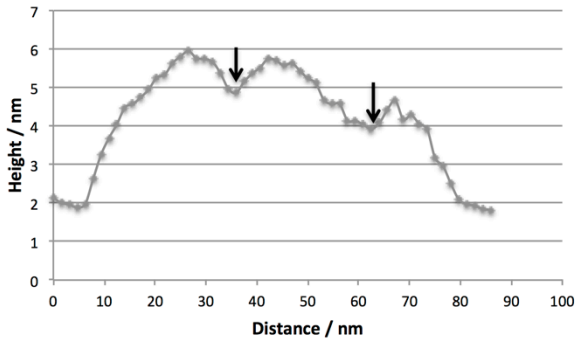

b)

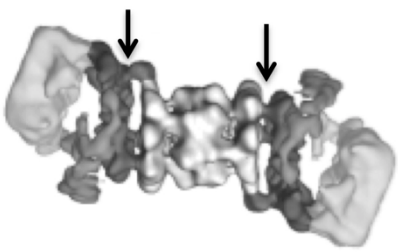

Figure 1. Distribution analysis of AFM data of 26S proteasome.
a) Intensity distribution of 26S particle of AFM image.
b) Molecular model of 26S proteasome particle.

CO6-3 The Application of Cancer Immunotherapy for the combination with Boron Neutron Capture Therapy (BNCT)

T. Suzuki, K. Horie, R. Abe, S. Masunaga[1], N. Kondo[1], Y. Sakurai[1], M. Suzuki[1] and K. Ono[1]

Recerch Institute of Biomedical Sciences, Tokyo University of Science
[1]Research Reactor Institute, Kyoto University

Introduction

Boron neutron capture therapy (BNCT) is an attractive therapy for local tumor control in the treatment of brain tumor, melanoma, and so on [1,2]. However, some important issues are remained: the tumor-specific accumulation of highly concentrated boron, the real-time quantification of boron concentration in local tumor tissues, and the prevention of re-growth and metastasis of residual tumor cells after BNCT. Recently, much progress has been seen in tumor immunotherapy, and attracts many attentions of clinical researchers [3,4]. To achieve successful tumor regression, we try to establish the combination treatments with BNCT and immunotherapy. Using the radiotherapy with X ray irradiation, we firstly examined the anti-tumor effect of the combination therapy.

Results and Discussions

The establishments of cancer immunotherapy

In last year, we established some immunotherapies, e.g. blockade of immunological checkpoints with anti PD-1mAb and/or anti CTLA-4 mAb, vaccination with dendritic cells (DCs), and adoptive cell transfer therapy (ACT), using mouse model. Until now, we investigated the mechanisms of potent anti-tumor immune response by ACT under lymphopenic condition [5,6]. Assessing anti-tumor effect by anti PD-1 mAb or anti CTLA4 mAb, we confirmed the anti-tumor effect by blockade of immunological check points (Fig.1). In addition, similar to clinical trials, we found that anti-tumor effect was not sufficient for the tumor regression in some mice, whereas few mice treated with mAb could reject tumors. Using this protocols, we assessed whether anti-tumor effect is enhanced by the combination with radiotherapy.

Anti-tumor effect by the combination with radiotherapy and immunotherapy.

To assess the effect of combination therapy with radiotherapy and immunotherapy, tumor bearing mice were treated by mAb, and were locally irradiated by X ray (12Gy). Expectedly, significant tumor regression was observed in mice treated with the combination therapy (Fig.2). Analyzing anti-tumor immune response, we found that the induction of tumor antigen specific CTLs was not augmented by combination therapy, whereas local X ray irradiation lead to the increase of CTL population. Notably, compared with prior-treatment, later administration of mAb could not lead to significant anti-tumor effect during combination therapy, suggesting that the appropriate timing of mAb treatments is important for the induction of strong anti-tumor effect during the combination therapy. Based on these observation, now, we are trying to establish the effective combination therapy with BNCT and immunotherapy.

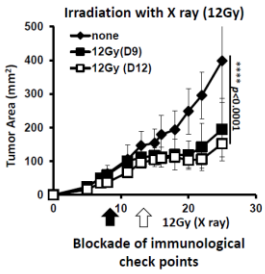

Figure 1. Anti tumor effect by single treatment, X ray or the blockade of immunological check point. 1x 10⁶ LLCgp33 cells, Lewis lung carcinoma expressing gp33 model antigen stably, were transplanted intra-dermally on right leg. Until 5 to 12 days after tumor inoculation, mice were treated by the radiotherapy with 12Gy local X ray irradiation (upper graph) or the immunotherapy with anti CTLA-4 mAb (lower left graph), and anti PD-1 mAb (lower right graph). Tumor growth was assessed by the tumor area. The *p* values in the graphs indicate the statistical significance of the difference between no-treatment and each treatment group.

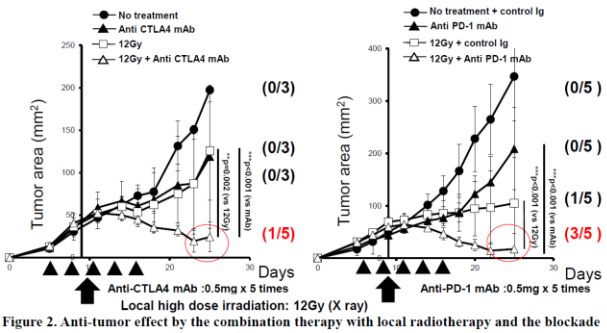

Figure 2. Anti-tumor effect by the combination therapy with local radiotherapy and the blockade of immuno-logical check points. 1x 10⁶ LLCgp33 cells were transplanted on right leg. Until 5 to 11 days, mice were treated by the immunotherapy with anti CTLA-4 mAb (left graph) and anti PD-1 mAb (right graph). Some mice were locally irradiated by 12Gy X ray, and tumor growth was assessed by the tumor area. The *p* values in the graphs indicate the statistical significance of the difference between each single treatment and combination therapy. Figures in the right of growth curve show the number of tumor rejected mice per total mice in each treatment group.

REFERENCES:

[1] M. Suzuki, *et al.* Int. J. Radiat. Oncol. Biol. Phys. 58(3): 892-896, 2004.
[2] M. Suzuki, *et al.* Int. J. Radiat. Oncol. Biol. Phys. 60(3): 920-927, 2004.
[3] Lifu Dengu *et al.*, *J. C. I.*, 124 (2), 687, 2014.
[4] M. A. Curran *et al.*, PNAS, 107(9), 4275, 2010.
[5] Suzuki T. *et al*, J. Immonol. 180:4596-4605, 2008
[6] Suzuki T. et al, Cancer Immunol. Immun. 65(3): 341-345, 2016

CO6-4 Development of Experimental Techniques for Neutron Biology

T. Chatake, S. Fujiwara[1], Y. Yanagisawa[2] and I. Tanaka[3]

Research Reactor Institute, Kyoto University

[1]National Institute for Quantum and Radiological Science and Technology

[2]Department of Pharmacy, Chiba Institute of Science

[3]Department of Technology, Ibaraki University

INTRODUCTION: Recent neutron source had achieved rapidly advancing development in a quarter century. Especially, the pulsed neutron source at J-PARC had enabled us various neutron experiment, which could never been carried out due to lower neutron beam from neutron reactor. In the present project, the following the forefront experiments were studied for neutron biology. (1) D/H contrast neutron protein crystallography (Fujiwara) (2) The combination of scattering experiments of physiologically active substances derived from Bacillus subtilis *natto* (Yanagisawa), and (3) Dynamic neutron polarization technique for neutron protein crystallography (Tanaka). Here, the results of (1) and (2) are reported.

(1) D/H contrast neutron protein crystallography

EXPERIMENTS: Bovine pancreatic ribonuclease A (Sigma) was used for this study. Crystallization was carried out in H_2O-solvent crystallization solution, in the similar manner as reported earlier [1]. The obtained H_2O-solvent crystal (h-crystal) was converted to D_2O-solvent crystal (d-crystal) by vapor diffusion method. Neutron diffraction data sets both of d- and h- crystals were collected using BIX-3 diffractometer at JRR-3M nuclear reactor. So far, the contrast between D and H atoms was calculated in reciprocal space [2]. On the other hand, we designed another calculation method (real space D/H contrast method), and developed software for real space D/H contrast method. This method was applied for the two neutron data sets of the d- and h- crystals at 1.8 Angstrom [3].

RESULTS: The real space D/H contrast maps provided detailed pictures of the H/D exchangeable atoms in ribonuclease A and its hydration with two superior properties to the previous D/H contrast method. (i) all of the observed amplitudes can be used to visualize the D/H contrast, while only the amplitude commonly observed in both d- and h- crystals can be used in the previous method. (ii) real space D/H contrast map can be easily incorporated into standard neutron crystallography. These advantages contributed to interpretations of the 3D structure of this protein including hydrogen atoms with high accuracy.

Solvent region was also investigated using D/H contrast map. Fig. 1 shows average density in the D/H contrast map along the distance from protein surface, where the surface is accessible surface area. The results strongly suggested the 1st hydration shell present 1.4-1.6 Angstrom apart from the protein surface, and the density shape likes a donut with the width of ~1.2 Angstrom. The further analysis of the hydration structure is in progress.

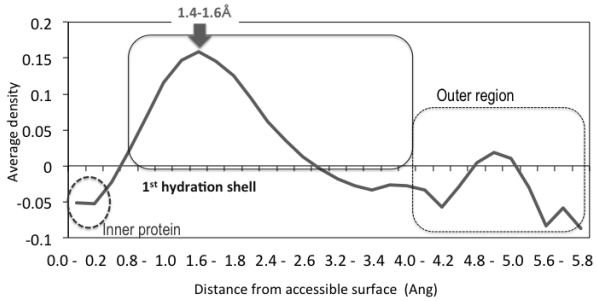

Fig. 1. Density of solvent region in D/H contrast map.

(2) Combination of scattering experiments of physiologically active substance derived from Bacillus subtilis *natto*

EXPERIMENTS: Bacillus subtilis *natto* secrets abundantly water soluble vitamin K_2 (MK-7). The chemical and structural compositions of MK-7 have not been determined, while MK-7 has been sold as supplements. Our aim of this project is to elucidate structural composition by the combination of scattering method (DLS, XANS, and SANS). The scattering method requires MK-7 of high quality and quantity. In this physical year, procedure of purification was improved to achieve purification of MK-7 with the highest quality ever.

RESULTS: 20 mM Tris-HCl (pH7.6) buffer was used through purification. 1 L of Cultured medium was filtered and concentrated to 17.2 mL volume containing 0.3 M NaCl before purification as described before [4]. 1st purification was carried out DEAE FF (5mL) (direct injection) with gradient of 0.3 M -> 1.0 M NaCl. The main fraction was further purified using the 2 times of DEAE FF (1mL) with the same gradient. After ion-exchange chromatography, gel-filtration chromatography was carried out using sephacryl S-200 (ϕ16x60cm). At the first gel-filtration, two peaks were observed in the elution curve. The former peak was collected and, they were purified in the same gel-filtration again.

Finally, 891 uL solution of purified MK-7 could be obtained. UV_{280nm} was 0.500. Bradford assay, in which BSA was used as standard, indicated 0.087 mg/mL protein was contained in MK-7. DLS and XANS are scheduled now.

REFERENCES:

[1] Berisio, R., Lamzin, V. S., Sica, F., Wilson, K. S., Zagari, A. & Mazzarella, L. *J. Mol. Biol.* **292**, 845–854 (1999).

[2] Kossiakoff, A. A., Sintchak, M. D., Shpungin, J. & Presta, L. G. *Proteins* **12**, 223–236 (1992).

[3] T. Chatake, S. Fujiwara, *Acta Crystallogr.* **D72**, 71-82 (2016).

[4] Y. Yanagisawa, M. Sakanushi, M. Ishiyama, S. Onuma, S. Fujiwara, T. Matsuo, T. Chatake, Y. Morimoto, KUR Progress Report 2013,P5-4 (2014).

CO6-5 Design and Synthesis of Boron-containing Compounds for Effective Accumulaion in Tumor Tissues and Detection by Boron Magnetic Resonance Imaging

S. Aoki, Y. Nishiura, T. Tanaka, Y. Hisamatsu, Y. Sawamoto, R. Araki[1], T. Saido[2], T. Suzuki[3], K. Horie[3], R. Abe[3], S. Masunaga[4], K. Natsuko[4], Y. Sakurai[4] and K. Ono[4]

Faculty of Pharmaceutical Sciences, Tokyo University of Science

[1]*Bruker Biospin K. K.*

[2]*RIKEN Brain Science Institute*

[3]*Research Institute of Biomedical Sciences, Tokyo University of Science*

[4]*Research Reactor Institute, Kyoto University*

INTRODUCTION: Boron neutron capture therapy (BNCT) is one of powerful therapies for local tumor control in the treatment of brain tumor, melanoma, and so on [1]. Some critical issues are remained for the successful BNCT, such as the tumor-specific accumulation of highly concentrated boron and the real-time detection of boron concentrations in local tumor tissues. In this study, we have designed and synthesized new boron compounds appended with glucose moiety and metal chelators for BNCT and B NMR (nuclear magnetic resonance) or MRI (magnetic resonance imaging) [2].

As for the boron compounds for more efficient accumulation in tumor tissues, we have synthesized several glucose-based boron compounds and assessed their tumor/blood (T/B) ratios [3].

As for B-MRI, some icosahedral carboranes derivartives, **1** and **2**, which are composed of 10 boron atoms and 2 carbon atoms and has considerable thermal and chemical stability, were synthesized (Fig. 1). We discovered the first example of full deboranation reaction of o-carborane catalyzed by d-block metal ions under physiological conditions [4]. Among various d-block metals tested, Cu^{2+} accelerates most efficiently to produce 10 $B(OH)_3$ from one molecule of carborane deriva-tives.

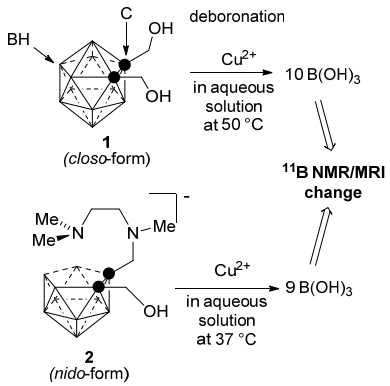

Fig 1. Deboronation reaction of carborane derivatives **1** and **2**, induced by Cu(II) in aqueous solutions.

EXPERIMENTS and RESULTS:

Tumor accumulation of boronyl glucose compounds. Low toxicity of the synthesized compounds were confirmed by animal tests. Although the distribution of these agents in tumor cells are low, it was found that T/B ratios of some compounds are 2.3~2.4, which is better than that of BSH (0.5) [3].

^{11}B NMR and MRI change of carborane derivatives by decomposition reaction promoted by copper(II).

Decomposition reaction of **1** and **2**, as well as our previous compounds [5] were followed by ^{11}B NMR and MRI. Interestingly, the probe **2** undergoes faster decomposition than that of **1** at 37 ºC and neutral pH, which was successfully detected on ^{11}B NMR and MRI (Fig. 2) [4,6].

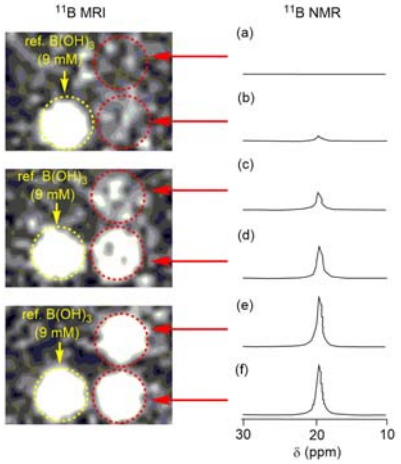

Fig 2. ^{11}B MRI and ^{11}B{^{1}H} NMR (128 MHz) spectra of **2** (2 mM) in DMSO/0.5 M HEPES (pH 7)/D_2O after incubation at different concentrations ((a)~(f) 0, 0.02, 0.1. 0.2 mM, 1.0, and 2.0 mM) of Cu(II).

REFERENCES:

[1] a) R. F. Barth *et al.*, *Clin. Cancer Res.*, **11** (2005) 3987-4002. b) R. F. Barth et al. *Rad. Oncol*. **7** (2012) 146-166.

[2] a) G. W. Kalbalka, et al. *J. Neuro-Oncol*. **33** (1997) 153-161. b) P. Bendel, *NMR in Biomed.* **18** (2005) 74-82.

[3] Y. Sawamoto, master thesis, Tokyo University of Science (2016)

[4] T. Tanaka *et al.*, *Eur. J. Inorg. Chem*. 1819-1834 (2016).

[5] M. Kitamura *et al.*, *Inorg. Chem.* **50** (2011) 11568-11580.

[6] T. Tanaka et al., *Eur. J. Inorg. Chem.* in press (2016)

CO6-6 Measurement of Transmittance Spectra of a Cryo-Sectioned Tissue of Brain Tumor C6 Model in the Sub-Terahertz Reagion-III

T. Takahashi and N. Miyoshi[1]

Research Reactor Institute, Kyoto University
[1] Research Center for Development of Far-Infrared Region, University of Fukui

INTRODUCTION: The accelerator-based radiation source in the millimeter and terahertz wave region has very attractive feature for the spectroscopy. Coherent transition radiation (CTR), which has been emitted from the short bunches of electrons at the KURRI-LINAC, has been used to observe the transmittance spectra of a sectioned tissue of raw brain tumor C6 model as a collaborate study in the research reactor institute, Kyoto university. The absorption spectra in the sub-terahertz region had been not so clear for the raw tumor tissue although Ashworth-PC. *et al*. [1] had reported for the excised human breast cancer by a terahertz pulsed spectroscopy observed at 320 GHz, which was estimated a longer relaxation time component of the induced electricity for water molecules [2-3] in the raw tumor tissue for three years at the linear analysis.

We also estimated what kind of water molecules become dominant in the viable and necrotic cancer regions by the different measurement method as an aim of 2D mapping study.

EXPERIMENTS: **(1)** Instrument of Near-field in tera-hertz region: The experiment was performed at the coherent radiation beamline [4] at the 40-MeV L-band linac of the Research Reactor Institute, Kyoto University. The width of the macro pulse and the repetition rate of the electron beam were 47 ns and 60 Hz, respectively. The charge of a bunch was 1.5 nC. The THz-wave source was CTR emitted from an aluminum foil with 15-μm thickness. The radiation was detected by a liquid helium cooled Si bolometer. The conical cone with an aperture 260 μm in diameter was used as the illumination probe and its F-number was 2.5. The spectrum of CTR was measured by a Martin-Puplett type interferometer. The schematic diagram of the experiment was shown in Fig.1.

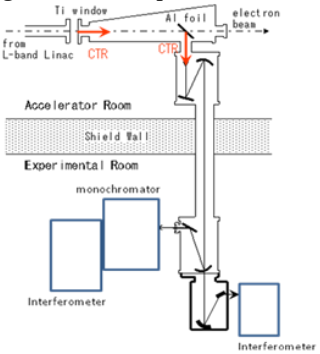

Fig.1 The schematic diagram of the experiment.

(2) Sample preparation: A cryo-sectioned (thickness=100 μm) tissue was prepared from the raw C6 glial tumor model using a Cryo-section Maker (Leica) and was sealed sandwich-type with saran-wrap film (thickness=10 μm), under freezing condition (-20 C) before the measurements.

RESULTS: The photograph of the cryo-sectioned tissue with the measurement points was shown in Fig.2. The spectra were measured at every point. The 2-dimensional imaging of the observed intensity at the wavenumber of 19 cm^{-1} was shown in Fig.3. The comparison between the spectral image and the H.&E.-stained Image is now progressing.

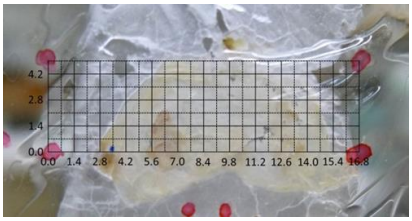

Fig.2 The photograph of the cryo-sectioned tissue with the measurement points.

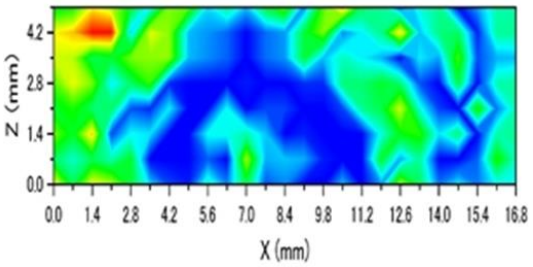

Fig.3 The 2-dimensional spectral imaging at the wavenumber of 19 cm^{-1}.

REFERENCES:

[1] Phillip C. Ashuworth, *et. al*., *Optics Express*, **17(14):** 12444-12454 (2009).
[2] Toshiko Fukasawa, *et al*., *Phys. Rev. Let.*, **95:** 197802 (2005).
[3] Hiroyuki Yada, *et al*., *Chem. Phys. Let.*, **464:** 166-170 (2008).
[4] T. Takahashi, *et al.*, Rev. Sci. Instrum. **69** (1998) 3770.

CO6-7 Protein Profiling and Drug Delivery on Cellular Apoptosis in Human Vitreous

T. Hisatomi, T. Tachibana, T. Ishibashi and N Fujii[2]

Graduate School of Medical Sciencesm
Kyushu University,
[1]*Graduate School of Science, Kyoto University*
Research Reactor Institute, Kyoto University

INTRODUCTION: Protein profiling in human vitreous may change in various vitreoretinal diseases. Regmatogenous retinal detachment is a severe retinal disease due to massive loss of retinal photoreceptors. Photoreceptor loss is mainly caused via molecular cascade to apoptosis. During this process, many proteins are released or accumulated in vitreous. Since photoreceptor apoptosis is initiated by activation of P2X7 receptor, P2X7 receptor blocker, brilliant blue G (BBG) may have therapeutic effects on retinal detachment. In this study, we examined protein profiling and drug delivery in human vitreous samples obtained during vitreous surgeries.

EXPERIMENTS:
Human vitreous samples are examined by HPLC and the results are compared between controls and various diseases. BBG concentration was analyzed with LC.

RESULTS:
The analysis showed major reported vitreous protein in human samples. The time-dependent changes of BBG are also observed by LC. The BBG concentration in eye and blood was also compared in the dose-dependent manner. Further studies are needed for detailed analysis in vitreoretinal diseases.

REFERENCES:

1)Notomi S, Hisatomi T, Kanemaru T, Takeda A, Ikeda Y, Enaida H, Kroemer G, Ishibashi T.
Critical Involvement of Extracellular ATP Acting on P2RX7 Purinergic Receptors in Photoreceptor Cell Death. Am J Pathol. 2011 Dec;179(6):2798-809.

2)Notomi S, Hisatomi T, Murakami Y, Terasaki H, Sonoda S, Asato R, Takeda A, Ikeda Y, Enaida H, Sakamoto T, Ishibashi T.
Dynamic increase in extracellular ATP accelerates photoreceptor cell apoptosis via ligation of P2RX7 in subretinal hemorrhage. PLoS One. 2013;8(1):e53338.